

Soft Matter

Accepted Manuscript



This is an *Accepted Manuscript*, which has been through the Royal Society of Chemistry peer review process and has been accepted for publication.

Accepted Manuscripts are published online shortly after acceptance, before technical editing, formatting and proof reading. Using this free service, authors can make their results available to the community, in citable form, before we publish the edited article. We will replace this *Accepted Manuscript* with the edited and formatted *Advance Article* as soon as it is available.

You can find more information about *Accepted Manuscripts* in the [Information for Authors](#).

Please note that technical editing may introduce minor changes to the text and/or graphics, which may alter content. The journal's standard [Terms & Conditions](#) and the [Ethical guidelines](#) still apply. In no event shall the Royal Society of Chemistry be held responsible for any errors or omissions in this *Accepted Manuscript* or any consequences arising from the use of any information it contains.



Journal Name

ARTICLE TYPE

Cite this: DOI: 10.1039/xxxxxxxxxx

Anisotropic Reversible Piezoresistivity in Magnetic-Metallic/Polymer Structured Elastomer Composites: Modelling and Experiments

José Luis Mietta,^a Pablo I. Tamborenea^b, and R. Martin Negri^{*a}

Received Date
Accepted Date

DOI: 10.1039/xxxxxxxxxx

www.rsc.org/journalname

Structured elastomeric composites (SECs) with electrically conductive fillers display anisotropic piezoresistivity. The fillers do not form string-of-particles structures but pseudo-chains formed by grouping micro-sized clusters containing nanomagnetic particles surrounded by noble metal (e.g. silver, Ag). The pseudo-chains are formed when curing or preparing the composite in the presence of a uniform magnetic field, thus pseudo-chains are aligned in the direction of the field. The electrical conduction through pseudo-chains is analyzed and a constitutive model for the anisotropic reversible piezoresistivity in SECs is proposed. Several effects and characteristics, such as electron tunnelling, conduction inside the pseudo-chains, and chain-contact resistivity are included in the model. Experimental results of electrical resistance, R , as function of the normal stress applied in the direction of the pseudo-chains, P , are very well fitted by the model in the case of Fe_3O_4 -[Ag] microparticles magnetically aligned while curing in polydimethylsiloxane, PDMS. The cross sensitivity of different parameters (like the potential barrier and the effective distance for electron tunnelling) is evaluated. The model predicts the presence of several gaps for electron tunnelling inside the pseudo-chains. Estimates of those parameters for the mentioned experimental system under strains up to 20% are presented. Simulations of the expected response for other systems are performed showing the influence of Young's modulus and other parameters on the predicted piezoresistivity.

1 Introduction

Structured Elastomer Composites (SECs) are formed by fillers anisotropically dispersed in an elastomer matrix. If the fillers are magnetically active, a simple procedure to obtain SEC materials is to cure the filler-elastomer composite in the presence of a uniform magnetic field, $\mathbf{H}_{\text{curing}}$. This process induces agglomeration of the filler particles into chain-like structures, referred to as pseudo-chains, aligned in the direction of $\mathbf{H}_{\text{curing}}$.¹⁻⁴ If, additionally, the filler particles are electrically conductive, the SECs may be conductors. These systems present piezoresistivity

(change of the electrical resistance, R , with an external mechanical stress, P) and/or magnetoresistivity (change of R with an external magnetic field), finding applications in sensors, flexible devices and electronic connectors.⁵⁻⁷ Piezoresistivity of iron particles in elastomers with relatively low crosslinking degree and PDMS-nickel particles loaded up to 30% v/v has been reported in low range of strains (up to 2.5%).⁸⁻¹⁰ In those systems, fillers are organized as strings of spherical particles, without internal structure. In the present study we consider completely different structures: magnetic nanoparticles form clusters and several of these clusters are surrounded by metallic silver (or any other noble metal) forming microparticles, which, in turn, are grouped by $\mathbf{H}_{\text{curing}}$ forming pseudo-chains. The theoretical modelling of the piezoresistivity generated by these structures is tackled here for the first time. The modelling of our systems formed by pseudo-chains requires consideration of the length, diameter, and rela-

^a Instituto de Química Física de Materiales, Ambiente y Energía (INQUIMAE), Departamento de Química Inorgánica, Analítica y Química Física, Facultad de Ciencias Exactas y Naturales, Universidad de Buenos Aires, Argentina. Fax: xx54-11-4576-3341; Tel: xx54-11-4576-3358; E-mail: rmn@qi.fcen.uba.ar

^b Departamento de Física and Instituto de Física de Buenos Aires (IFIBA), Facultad de Ciencias Exactas y Naturales, Universidad de Buenos Aires, Argentina

tive orientation of the pseudo-chains. Also, factors like the electrical resistance of the microparticles must be accounted for in our model, while filler particles are currently considered as perfect conductors.⁹ Additionally, in string-of-particles systems some specific parameters must be previously estimated^{8–10}, such as the thickness of the polymer layer between particles and the number of electron tunnel steps. It appears that string-of-particles systems can be more easily formed in matrices with relatively low degree of cross-linking, displaying large piezoresistivity at relatively low strains. On the other hand, systems where pseudo-chains are formed (instead of string of particles) and strains larger than 5% are considered, require a different theoretical approach.

As mentioned above, the fillers used in our previous works are simultaneously magnetic and conductive.^{1,5–7,11} First, magnetic nanoparticles (NPs) in the superparamagnetic regime are synthesized. The superparamagnetic regime is required in order to avoid irreversibility in the magnetic response for magnetoresistivity applications and is obtained by synthesizing NPs with diameters below a given critical size (e.g. Fe_3O_4 of 10–20 nm are in the superparamagnetic state at room temperature). These NPs form agglomerates because of the magnetic interactions. Then, the agglomerates are covered with silver (Ag), generating microparticles (referred as μPs) which are simultaneously superparamagnetic and electrically conductive. These μPs are dispersed in the elastomer and then cured in the presence of $\mathbf{H}_{\text{curing}}$. In this way, several μPs form one pseudo-chain. The anisotropic structure induces anisotropic elastic^{4,12}, magnetic¹³ and electrical^{1,5} properties. Because of many factors involved while curing, such as local magnetic interactions between μPs in directions which are not parallel to $\mathbf{H}_{\text{curing}}$, hindrance for particle drifting in the matrix and head-to-tail interactions between chains while they are generated, pseudo-chains are not perfectly aligned in the direction of $\mathbf{H}_{\text{curing}}$ but rather an angular distribution is obtained. Pseudo-chains appear forming columns, one after the other, with a small angle between them, since the angular standard deviation, σ_θ , is narrow when using relatively high intense fields and strong magnetic compounds ($\sigma_\theta \leq 4^\circ$ for systems described in previous works).^{11,14} Electron transport through these columns allows the observation of anisotropic electrical conduction in SECs. One important aspect of modelling that process is the discrimination between consecutive pseudo-chains. Pseudo-chains appear as oblong structures, thicker at the centre and thinner at the ends. Therefore, a given pseudo-chain is distinguished from the consecutive one by the two mentioned characteristics: the small angle between the pseudo-chains and the observation of a thinning at the end-beginning of each one. Pseudo-chains present also a certain length distribution, with average $\langle \ell \rangle$, observed by SEM. The average diameter of a pseudo-chain is indicated by $\langle D \rangle$.

Finally, we call the reader's attention to the internal structure of the pseudo-chains, which presents not only irregularities in the

arrangement of the μPs , but also gaps due to polymer penetration.^{15,16} That is, pseudo-chains are not compact structures (the internal structure is not represented in schemes like Figure 1, for simplicity).

By setting the experimental conditions (filler concentration, $\mathbf{H}_{\text{curing}}$, degree of cross-linking, etc.) it is possible to obtain electrical conduction only in the direction of $\mathbf{H}_{\text{curing}}$ (no measurable conduction in the orthogonal direction). This situation is referred to here (and in a previous work⁷) as Total Electrical Anisotropy (TEA). TEA is a crucial property in devices like extended pressure mapping sensors^{1,5,7} and Zebra[®]-like connectors for parallel flip-chip connections. Actually, most of the SECs previously prepared and characterized in our group present TEA. These systems display reversible piezoresistivity when applying a normal stress, P , in the direction of $\mathbf{H}_{\text{curing}}$. That is, the electrical resistance of the SEC in the direction of $\mathbf{H}_{\text{curing}}$, R , decreases by applying a normal stress P in that direction. Reversible piezoresistivity is the other key factor for developing devices and sensors, not always present in similar systems.^{9,17–19} Thus, the main objective of this work is to present a constitutive model which accounts for the observed piezoresistivity of SECs under TEA conditions and to simulate the predictions of the model for different materials and experimental conditions.

2 Materials and Methods

The synthesis and characterization of several magnetic NPs (magnetite, nickel, cobalt ferrites) has been extensively reported in our previous works.^{1,2,5,6} They were used as fillers dispersed in elastomer matrices like polydimethylsiloxane (PDMS) and styrene-butadiene-rubber (SBR). The model developed in the present work applies to all of these systems under TEA condition. One of the SECs used in previous works ($\text{Fe}_3\text{O}_4[\text{Ag}]\text{-PDMS}$ 4.2% v/v) is taken here as a reference material to show connections between theoretical parameters and experimentally observed magnitudes. In this work, PDMS refers to the unfilled elastomeric matrix formed by a base:cross-linker of 10:1 weight ratio. The mixture is homogenized, degassed and placed (while still fluid) inside a cylindrical mould for curing. The mould is part of a designed device which allows the thermal curing of the samples in the presence of $\mathbf{H}_{\text{curing}}$, while rotating the sample at a constant speed (using a motor and a circular strap) for homogenizing and prevent settling of the filler. After curing and de-moulding, samples of cylindrical shape (typical diameter about 10 mm) are cut using a specially designed device to obtain pieces of thickness L_o about 2–3 mm. A scheme of the internal structure of the SECs is shown in Figure 1.

The number of quasi-aligned columns, N , formed by several pseudo-chains is estimated using SEM images in cross-sections of the SECs, recorded with a field emission scanning electron microscope (FESEM, Zeiss Supra 40 Gemini) at several magnifications

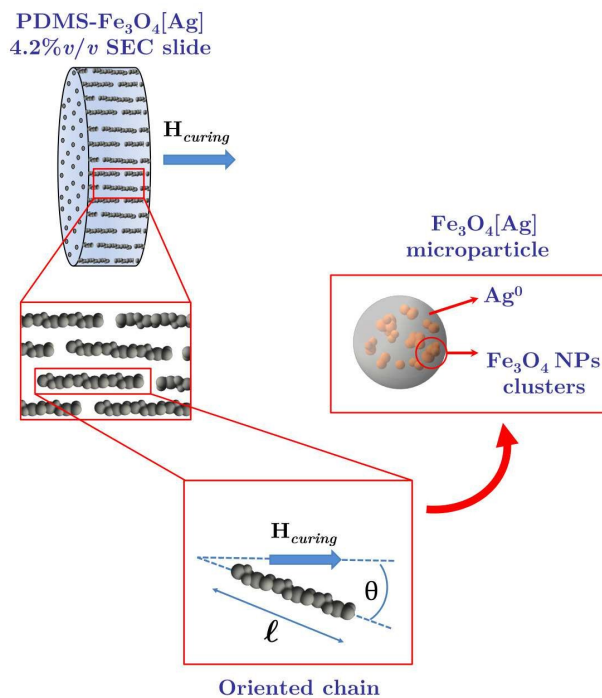


Fig. 1 Scheme of the internal structure of a SEC sample. Each pseudo-chain is formed by several magnetic-metallic microparticles (μ Ps).

(from 50 to 6000 \times) and voltages (EHT) of 3 to 5 kV. The elastic behaviour is investigated with a Stable Microsystems TA-XT2i texture analyser, which compresses the samples at a constant speed ($100 \mu\text{s}^{-1}$) up to a final strain (about 20–40% in the case of the filled PDMS samples). For piezoresistance measurements, the SEC samples are placed between two gold electrodes and connected to a potentiostat (TEQ 4, Argentina) symbolized by an ammeter and variable voltage source in Figure 2. The normal stress is applied by a worm screw (in orthogonal position with respect to the sample surface) and measured with an electronic balance (force sensor). The electric potential-current characteristic curve is recorded (dc, typically between ± 3 V) for each applied stress.

3 Electrical resistance for conductive columns formed by quasi-aligned pseudo-chains

Pseudo-chains are aligned in the direction of $\mathbf{H}_{\text{curing}}$, with a small angular dispersion. It is assumed that there are columnar structures, formed by several pseudo-chains, which run across the SEC. It is assumed also that there are N of those columns, all of them

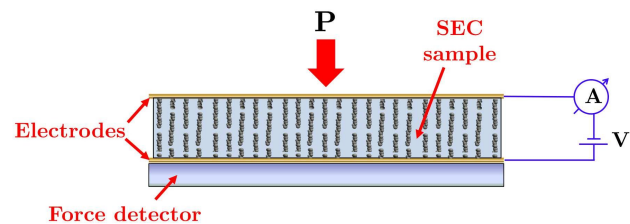


Fig. 2 Scheme of the experimental set-up for measuring piezoresistivity.

with the same electrical resistance, R_L . The number of columns, N , depends on specific experimental factors and the dimensions of the sample, and it usually falls in the range $10^2 - 10^3$.^{5-7,11} Actually, it must be distinguished between *Local Conductive Clusters*, *LCC* and *Effective Conductive Clusters*, *ECC* when determining N .¹⁸ The ECCs extend from one electrode to the opposite contributing to the electrical conductivity of the material, while the LCCs are located within the SEC material, touching one or none of the electrodes, and do not contribute to the electrical conductivity (behaving as isolated conductor elements). In this work it is assumed that $N_{\text{ECC}} = N$. It is also assumed that there is no creation/destruction of ECCs during compression.

Each column makes electrical contact with the electrodes, with a contact resistance R_{E-CH} (considered the same at the top and bottom electrodes and equal for each column). Current lines perpendicular to the columns are neglected because of the high electrical resistivity of the polymer matrix (about $10^{14} \Omega\text{cm}$ in the case of PDMS).²⁰ That is, TEA is assumed. Thus, the total electrical resistance of the SEC, R , can be expressed in terms of an equivalent circuit of N parallel resistances, given by

$$R = \frac{2R_{E-CH}}{N} + \frac{R_L}{N} \quad (1)$$

The main term to be modelled is $\frac{R_L}{N}$. Although the contribution of the term $\frac{2R_{E-CH}}{N}$ can be taken into account explicitly in the model as a function of the applied stress, P , it will be shown that it is negligible. In fact, the contact electrical resistance between two conductive surfaces, represented here by one terminal pseudo-chain covered with metal (Ag in our case) and one gold (Au) electrode is modelled using the Holm model:²¹⁻²⁶ $R_{E-CH} \approx \frac{\rho_{\text{metal}} + \rho_{\text{Au}}}{4\alpha}$, where α is the radius of the cluster formed by spots that make effective contact between the two conducting surfaces (Holm radius), and $\rho_{\text{metal}} = \rho_{\text{Ag}}$. This expression is valid when the number of spots/surface irregularities making contacts between the SEC and the electrode is large, as is usually the case. The relationship between α and the stress P is provided by considering that^{24,27} $\pi\alpha^2 = \frac{F}{\mathcal{H}}$, where \mathcal{H} is the hardness of the softer contacting element (silver, the metal, in the present case). The contact force, F , is estimated by $F = P \times (\text{area of one column}) = P \times \left[\pi \left(\frac{D}{2} \right)^2 \right]$,

where $\langle D \rangle$ is the average diameter of one pseudo-chain. Thus, the model of Holm provides the following dependence of R_{E-CH} with P :

$$R_{E-CH}(P) = \frac{\rho_{metal} + \rho_{Au}}{2\langle D \rangle} \sqrt{\frac{\mathcal{H}}{P}} \quad (2)$$

R_{E-CH} is a decreasing function of the stress, P . Considering that the applied stresses for relatively high cross-linked SECs are commonly larger than 1 kPa ($P \geq 1$ kPa), and taking $\rho_{Au} = 2.4 \times 10^{-8} \Omega\text{m}$, $\rho_{Ag} = 1.6 \times 10^{-8} \Omega\text{m}$, $\mathcal{H} = \mathcal{H}_{Ag} = 250$ MPa (values at 20°C)²⁷ and $\langle D \rangle \sim 10 \mu\text{m}$, then $R_{E-CH} \leq 1 \Omega$ is predicted (for instance, $R_{E-CH} \approx 1 \Omega$ is estimated at $P = 100$ kPa). As the number of aligned columns formed by pseudo-chains, N , is typically in the order of $10^2 - 10^3$, then the contribution of the electrode-columns, $\frac{R_{E-CH}}{N}$, to the total resistance R is predicted to be in the range $(10^{-2} - 10^{-3}) \Omega$ which is about one or two orders of magnitude lower than the observed resistance R . Although Eq.(2) can be used for estimating the contribution of R_{E-CH} as function of P , it is clear that it is negligible. This can be confirmed by fitting the experimental data, $R(P)$, using the developed model.

Therefore, the next objective is to evaluate $\frac{R_L}{N}$ in Eq.(1). R_L has two contributions: the electron transport in regions of relatively high electron mobility inside a pseudo-chain and the barriers associated to gaps between regions. If R_{CH} represents the resistance in one zone of high electron mobility, n the number of such zones, R_{tunnel} the tunnelling resistance for crossing the barriers between those zones, and assuming the zones are perfectly aligned, then:

$$R_L = nR_{CH} + (n-1)R_{tunnel}(P) \quad (3)$$

The number n represents the number of gaps (in one column) between regions where the electron mobility is relatively high, separated by polymeric material. Thus, in a first approximation, it could be reasonable to consider these zones as one pseudo-chain, although the possibility of having gaps inside pseudo-chains is not discarded and actually accounted by the parameter n .

Concerning R_{CH} , the number of μPs of NPs-Ag is so high in a pseudo-chain (and also in a column) doing beyond the scope of the present study to develop a constitutive model for R_{CH} in terms of electrical resistances network conductivity. For instance, the number of μPs of NPs-Ag in one pseudo-chain, χ , can be estimated assuming a pseudo-chain of cylindrical shape with diameter $\langle D \rangle$ and length $\langle \ell \rangle$ formed by packaging χ microparticles of diameter $\langle D_{\mu P} \rangle$ with a packaging efficiency f . These magnitudes are related by: $\pi \left(\frac{\langle D \rangle}{2}\right)^2 \langle \ell \rangle f = \chi \frac{4}{3} \pi \left(\frac{\langle D_{\mu P} \rangle}{2}\right)^3$. χ can be estimated for the SEC used as reference in this work: $\langle D \rangle = 10.4 \mu\text{m}$, $\langle \ell \rangle = 1.3$ mm and $\langle D_{\mu P} \rangle = 1.3 \mu\text{m}$. For a close-packing of tetragonal repetitive units it is $f = 0.74$. However, the internal structure of the pseudo-chains is not close-packed. Taking $f = 0.5$ and $f = 0.74$ (a reasonable variation range) one obtains $\chi = 0.5 \times 10^5$ ($f = 0.5$) and $\chi = 8 \times 10^5$ ($f = 0.74$). In any case, it is clear that pseudo-

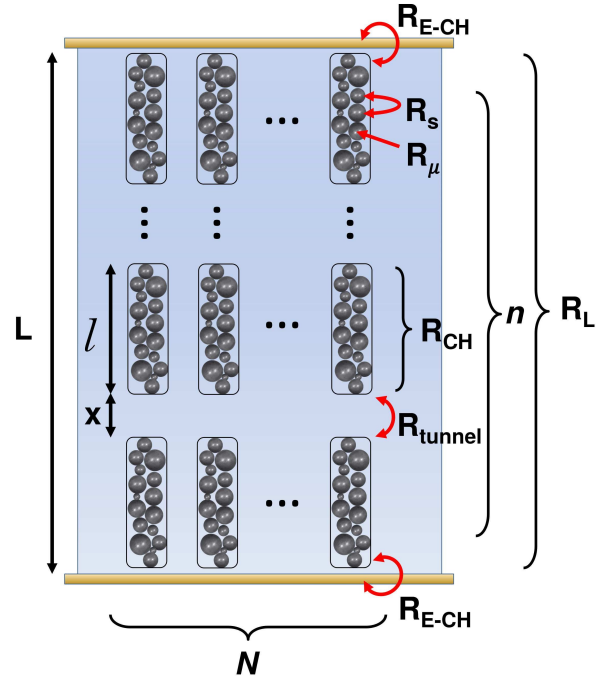


Fig. 3 Scheme illustrating the parameters of the model.

chains are formed by a large number of particles, making it difficult to estimate R_{CH} .

For all the above mentioned reasons, the parameters n and R_{CH} are considered independent of P and freely adjustable, to be recovered by fitting the experimental data. The parameters involved in Eqs. (1)-(3) are shown in Figure 3.

3.1 Electron tunnelling resistance, R_{tunnel}

R_{tunnel} in Eq. (3) is modelled in the present and next Sections. Note that the only considered mechanism for barrier-crossing is electron tunnelling since it is well-known that the electric conduction between two metal micrometric objects separated by a layer of insulating material (the polymeric matrix) is governed by electron tunnelling.²⁸⁻³² R_{tunnel} represents the electron tunnelling resistance between two adjacent conductive zones. It is considered here that the involved areas correspond only to the surfaces of the head and tail of two adjacent conductive regions. Its curvature is considered as approximately spherical with diameter given by the average diameter of the chains, $\langle D \rangle$.

The electron tunnelling between two flat conductive metallic surfaces for moderate electrical potential difference between the surfaces, V_{tunnel} , can be expressed using the Simmons' formalism.³³⁻³⁶ The two flat metallic surfaces are separated by an insulating layer of thickness x , where a rectangular potential barrier of height ϕ is present and image-force effects are neglected.³⁶⁻³⁹

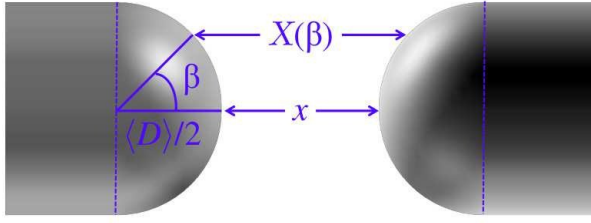


Fig. 4 Hemispherical surfaces of diameter $\langle D \rangle$ separated by a distance x . This surfaces correspond to the tail and head of two adjacent conductive regions.

Then, the electric current per unit area, J_{tunnel} is given, according to Simmons in the ohmic regime, by

$$J_{tunnel} = B \frac{\gamma}{x} \exp(-\gamma x) V_{tunnel} \quad (4)$$

In Simmons' formalism γ and B are given by³⁶

$$\gamma = \frac{4\pi}{h} \sqrt{2m\phi} \quad (5a)$$

$$B = \frac{3e^2}{8\pi h} \quad (5b)$$

where e is the electron charge, m is the effective electron mass in the filler material and h is the Planck constant.

However, it is necessary to generalize the result obtained by Simmons in order to include the case of two hemispherical surfaces. As shown in Figure 4, the separation between the hemispherical surfaces at the angle β is given by

$$X(\beta) = x + \langle D \rangle (1 - \cos \beta) \quad (6)$$

The electronic tunnel current between the two surfaces, I_{tunnel} , is obtained by integrating the current density in the direction of $\hat{\mathbf{X}}$, $\mathbf{J}_{\mathbf{X}}(X(\beta)) = J(X)\hat{\mathbf{X}}$:

$$I_{tunnel} = \iint_{\mathbf{G}} \mathbf{J}_{\mathbf{X}} \cdot d\mathbf{A} \quad (7)$$

where \mathbf{G} corresponds to the half-spherical surface and

$$\mathbf{J}_{\mathbf{X}} = B \frac{\gamma}{X(\beta)} \exp[-\gamma X(\beta)] V_{tunnel} \hat{\mathbf{X}} \quad (8)$$

The element $d\mathbf{A}$ can be expressed as a function of β by using spherical coordinates as $d\mathbf{A} = \left(\frac{\langle D \rangle}{2}\right)^2 \sin \beta d\phi d\beta \hat{\mathbf{r}}$, thus obtaining:

$$R_{tunnel} = \frac{V_{tunnel}}{I_{tunnel}} \quad (9)$$

$$R_{tunnel} = \frac{4}{\langle D \rangle^2 \int_0^{2\pi} d\phi \int_0^{\frac{\pi}{2}} \frac{B\gamma}{X(\beta)} \exp[-\gamma X(\beta)] \sin \beta \cos \beta d\beta} \quad (10)$$

or, in a more compact way:

$$R_{tunnel} = \frac{2}{\pi B \gamma \int_x^{x+\langle D \rangle} \frac{X-x}{X} \exp[-\gamma X] dX} \quad (11)$$

The parameter γ and the constant B in Eqs. (10) and (11) are considered to be given by Eq. (5a) and (5b). The integral in Eq. (11) does not have analytical solution⁴⁰ and was numerically evaluated using the Numerical Integration module of SageMath. The integral expression in Eq. (11) depends on the distance x which, in our model, is assumed to decrease with the applied stress, P . Therefore, the objective of the next Section is to model x as a function of P .

3.2 Modeling $x(P)$ - Mechanical characterization of the polymeric matrix

Since the Young's modulus of the filler is much higher than the Young's modulus of the elastomeric matrix, it is considered that the application of P does not introduce structural distortion of the conductive regions.

The parameter $x(P)$ is the average distance that the electrons must cross in one tunnel step. It could be reasonable in a first approximation to consider them as gaps between pseudo-chains. However, since pseudo-chains are complex structures where the groups of microparticles can be separated by polymer layers, these gaps can be present also inside pseudo-chains. It will be assumed that the polymer matrix layer separating two conductive regions has the same elastic behaviour as a macroscopic sample of the matrix polymer. This situation applies to relatively highly cross-linked systems, as those studied by our group and others. For instance, Ivaneyko *et al.*⁴¹ in studies of magneto-sensitive elastomers, have recently described a situation where the high cross-linking of composites prohibits a free movement of filler particles inside the polymer matrix but rather move affinely with it. This is the so-called *affine assumption*, which is assumed in the present work also since the considered SECs are relatively highly cross-linked. Effects of larger deformations of the matrix in the vicinity of very rigid fillers, as those described by Domurath *et al.*⁴² are not considered. Summarizing, in our model pseudo-chains follow the compression motion of the matrix when a stress is applied (actually, this implies that samples are incompressible). In other words, pseudo-chains are assumed to move along with the matrix. This assumption is mathematically expressed by

$$x(P) = x_o \lambda(P) \quad (12)$$

with $\lambda(P) \equiv \frac{y(P)}{y_o}$, where $y(P)$ and y_o are the thickness of a macroscopic unfilled matrix (e.g. pure PDMS) under a stress P and for $P = 0$, respectively. On the other hand, the parameter x_o is the gap separation for tunnelling in the SEC at $P = 0$.

Therefore, the model presented here requires expressions

for λ as function of P which must be introduced into the dependence of R with x using the affine assumption. The experimental variation of λ with P is obtained from uniaxial compression tests, as the one shown in Figure 5. In that figure, P represents the so-called *engineering stress*, $P = (\text{applied force}) / (\text{area in absence of applied force})$. The $P - \lambda$ dependence is commonly fitted using the Neo-Hooke (N-H) or the Mooney-Rivlin (M-R) models.^{43,44} These models provide expressions for P as function of λ that were used to fit the experimental data of Figure 5. The obtained results for each model are described here below.

Neo-Hooke model

The engineering stress, P , according to the Neo-Hooke model (and assuming the material does not change its volume; incompressible material) is given by:^{43,44}

$$P = 2C_1^{N-H} \left(\frac{1}{\lambda^2} - \lambda \right) \quad (13)$$

In the Neo-Hooke model the parameter C_1^{N-H} is related to the Young's modulus of the matrix by $C_1^{N-H} = E/6$.^{43,44} The Neo-Hooke model provides closed expressions for $\lambda(P)$ (which are actually the solutions of a cubic polynomial):

$$\lambda_j(\hat{P}) = a_j \xi(\hat{P}) - \hat{P} + b_j \frac{\hat{P}^2}{\xi(\hat{P})} \quad (14)$$

with

$$\xi(\hat{P}) = \frac{1}{2^{1/3}} \left[\sqrt{1 - 4\hat{P}^3} + 1 - 2\hat{P}^2 \right]^{1/3} \quad (15)$$

with $\hat{P} \equiv P/E$, $a_j = -\frac{1}{2}(i\sqrt{3}+1)$, $-\frac{1}{2}(-i\sqrt{3}+1)$, 1 and $b_j = -\frac{1}{2}(-i\sqrt{3}+1)$, $-\frac{1}{2}(i\sqrt{3}+1)$, 1 for $j = 1, 2, 3$ (i is the imaginary unit).

It is shown in Figure 5 that in the present case the Neo-Hooke model does not fit the experimental curve. Then, the Mooney-Rivlin model is considered.

Mooney-Rivlin model:

The expression for the engineering stress provided by the Mooney-Rivlin (M-R) model is:^{43,44}

$$P = \left(2C_1^{M-R} + \frac{2C_2^{M-R}}{\lambda} \right) \left(\frac{1}{\lambda^2} - \lambda \right) \quad (16)$$

Excellent fit of the experimental data was obtained in this case (see Figure 5) with $C_2^{M-R} = (711 \pm 4)$ kPa and $C_1^{M-R} = (-692 \pm 5)$ kPa. The M-R closed expressions for λ as function of P are solutions of a quartic polynomial. Although analytical expressions can be obtained in this case also⁴⁵, we decided to obtain numerical solutions and to use them into the expression for R [Eqs. (1)-(3), (6), (11)] through the proposed dependence of x with λ [Eq.(12)].

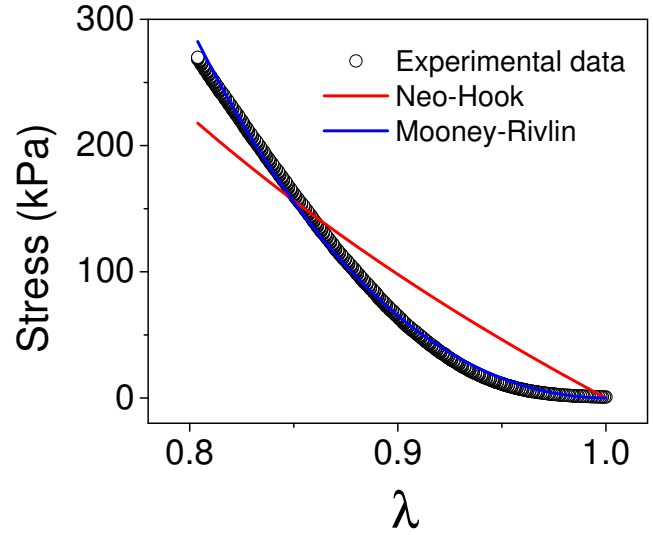


Fig. 5 Normal stress, P as function of λ ($P \equiv \frac{y(P)}{y_0}$), for a PDMS sample (base:cross-linker ratio = 10:1) non-loaded with filler particles. The red solid line corresponds to the Neo-Hooke model fit [Equation (13)] with $C_1^{N-H} = (146 \pm 1)$ kPa. The blue solid line corresponds to the Mooney-Rivlin model fit [Equation (16)] with $C_1^{M-R} = (-692 \pm 5)$ kPa and $C_2^{M-R} = (711 \pm 4)$ kPa.

Once $\lambda = \lambda(P)$ for the polymer matrix (not for the SEC) is introduced into the constitutive equations, the model can be used to fit experimental data of $R = R(P)$. In the present approach, this requires to determine also two morphological parameters of the SEC: the average number of columns in the considered sample, N , and the average diameter of a column (assumed equal to the diameter of a pseudo-chain, $\langle D \rangle$). Hence, the model has three parameters that are recovered by fitting, referred to as A_1 , A_2 and A_3 :

$$A_1 = \frac{(n-1)x_0}{B\gamma} \quad (17a)$$

$$A_2 = \gamma x_0 \quad (17b)$$

$$A_3 = \frac{n}{N} R_{CH} \quad (17c)$$

In Eq. (17a), the parameter B is a universal constant [see Eq. (5b)]. The parameters n and x_0 can be obtained from A_1 and A_2 in terms of γ . Eq. (5a) allows estimating γ if the tunnelling barrier ϕ and the effective electron mass, m , are known.

Equations (1)-(3), (6), (11), (12) and (16) represent the constitutive relationships of the present model. Fits of the experimental piezoresistivity data, $R = R(P)$, for the considered reference SEC are presented in the next section.

4 Fits of Experimental Results for the Reference SEC

The different SEC samples prepared in our group exhibit two relevant characteristics: anisotropic and reversible piezoresistivity.^{5-7,11} Regarding anisotropy, the experimental conditions can be optimized to obtain Total Electric Anisotropy (TEA), that is, conduction in one direction exclusively, as indicated in the Introduction.¹¹

The piezoresistive response is fully reversible (absence of piezoresistive hysteresis after hundred cycles of compression-decompression). The piezoresistive response of the material is not modified by bending or twisting of the sample in the direction perpendicular to the pseudo-chains.⁵⁻⁷ These results suggest that there are no irreversible changes in the internal architecture of the pseudo-chains. Thus, plastic deformation of the microparticles forming the chains is reasonably discarded.

There are two main factors that usually induce irreversibility in the piezoresistive response: (i) when fillers can move decoupled from the polymer matrix under the applied stress. This is not the case of the relatively high cross-linked composites considered here, as described in Section 3.2; (ii) if there were chemical bonds between filler-polymer. In that case, the bonds may be irreversibly broken during compression-decompression cycles, thus inducing hysteresis effects. This seems not to be the present case in our systems, as the observation of non-adhesion zones suggests that chemical bonds between pseudo-chains and matrix are not favoured (see Figure 6). These non-adhesion zones are not a consequence of the process of cutting material slides, as cryo-fragmentation of the material (where SEC samples were pre-cooled with liquid nitrogen and then cut) show non-adhesion filler-matrix zones also. Figure 6 shows SEM images that illustrate the most relevant morphological aspects of the SEC composites described here, including the presence of non-adhesion zones (Figure 6-a), the interpenetration of polymeric material within a pseudo-chain, and the grouping of microparticles in the pseudo-chains (Figure 6-b and c).

The linear I-V characteristic curves (not shown, measured as function of P) indicate that SECs exhibit ohmic behaviour over the whole range of applied electrical potentials and stresses. The inverse of the slopes of these curves are the values of $R(P)$, the electrical resistance measured at each applied stress (Figure 7).

The following procedure for obtaining and interpreting the microscopic variables is completely general. However, the values reported correspond to the reference SEC sample ($\text{Fe}_3\text{O}_4[\text{Ag}]$ -PDMS 4% v/v of filler material, 10:1 base:cross-linker ratio, $\mathbf{H}_{\text{curing}} = 0.3$ T, curing temperature: 80° C, exposition time: 4 hours, $L_o = 2.50$ mm). For that reference sample it was obtained $A_1 = (2.2 \pm 0.2) \Omega$, $A_2 = \gamma x_o = (11.1 \pm 0.5)$ and $A_3 = (0.47 \pm 0.07) \Omega$, with a good degree of adjustment ($\mathcal{R}^2 = 0.995$).

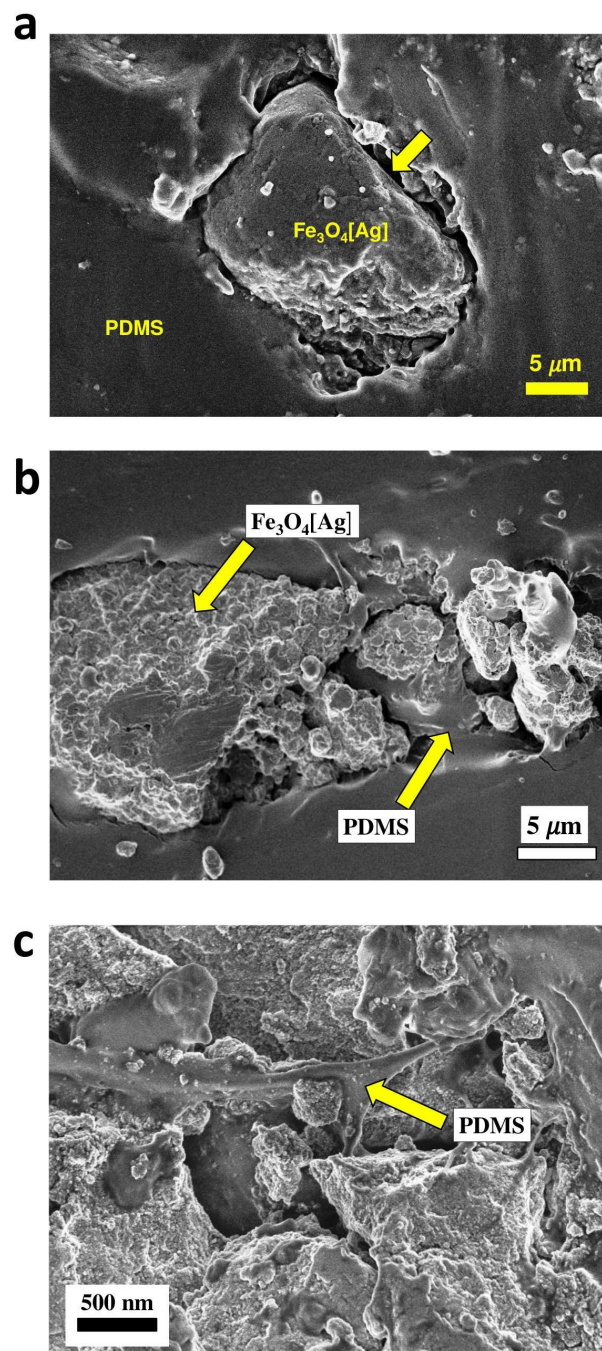


Fig. 6 SEM images of the $\text{Fe}_3\text{O}_4[\text{Ag}]$ -PDMS reference SEC. Panel (a) shows non-adhesion zones between pseudo-chains and the matrix. Panel (b) illustrates the interpenetration of the polymer within a pseudo-chain. Panel (c) is a magnification of panel (b).

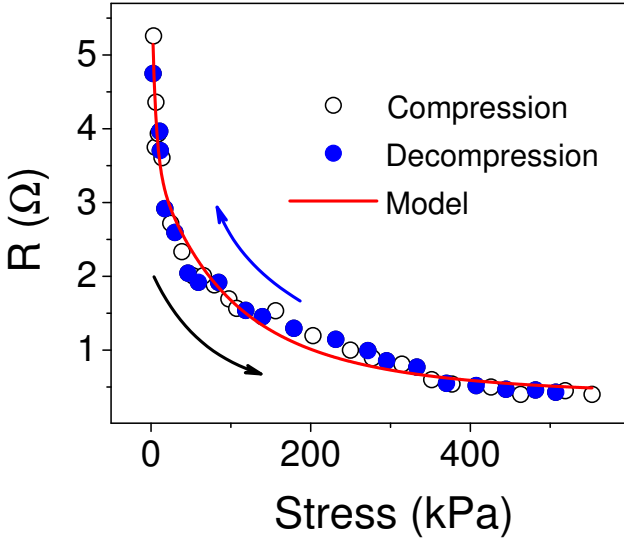


Fig. 7 Fits of the experimental electrical resistance, R , using the present model for the case of the reference SEC (see text). The solid red line corresponds to the model fit. Input parameters $\langle D \rangle = 10.4 \mu\text{m}$ and $N = 660 \pm 50$ were used. The thickness of the sample is $L_o = (2.50 \pm 0.01) \text{ mm}$.

As mentioned before, n and x_o can be calculated as a function of γ , which in turn is dependent on the tunnelling barrier, ϕ , and the effective electron mass, m . The barrier ϕ is obtained from measurements of the work function for the metal-insulator couple. For silver nanowires in PDMS it was recently reported $\phi = 1 \text{ eV}$.⁴⁶ Using that value of ϕ and the free electron mass, $m = m_e$ (conditions that are indicated by the upper symbol \dagger), it is obtained $\gamma^\dagger = 1.0 \times 10^{10} \text{ m}^{-1}$, $n^\dagger = (98 \pm 9)$ and $x_o^\dagger = (1.08 \pm 0.05) \text{ nm}$ for the reference SEC. $R_{CH}^\dagger = (3.2 \pm 0.3) \Omega$ is recovered using $N = (660 \pm 50)$. The values of n^\dagger and x_o^\dagger can be used to estimate the effective length of the highly conductive regions, l , that is the length of the regions between electron-tunnelling gaps, assuming:

$$L_o = (n - 1)x_o + nl \quad (18)$$

For the reference SEC sample is $L_o = (2.50 \pm 0.01) \text{ mm}$, that renders $l^\dagger = (26 \pm 4) \mu\text{m}$ which is about 50 times lower than the average length of pseudo-chain observed by SEM ($\langle \ell \rangle = 1.35 \text{ mm}$). This result is in agreement with the observation that pseudo-chains have micro-gaps caused by the interpenetration of polymer within and/or constrictions (narrowings) and irregularities as observed in Figure 6 b-c. These results are consistent also with the previous observation⁵ that the increase of the Young's modulus of the SEC, E , is lower than the prediction of the most commonly used models (such as the modified Halpin-Tsai model and the Hui-Shia model) when $\langle \ell \rangle$ is introduced in those models. Thus, the previously reported difference between observed and calculated values of E suggests the same conclusion that ob-

served here: the effective length of the pseudo-chains is predicted to be lower than $\langle \ell \rangle$.

The model allows estimating the contribution of each term in Eqs. (1)-(3) to the total electrical resistance, R . For example, for $P = 100 \text{ kPa}$ it is obtained $\left(\frac{n-1}{N}\right) R_{tunnel} \approx 1.17 \Omega$, $\left(\frac{2}{N}\right) R_{E-CH} \approx 3 \times 10^{-4} \Omega$, and $\left(\frac{n}{N}\right) R_{CH} \approx 0.5 \Omega$. At the highest stresses, R converges to the contribution made by the intrinsic resistance of chain structures, $\left(\frac{n}{N}\right) R_{CH}$. The recovered value of R_{CH} is higher than the associated to one continuous metallic silver chain, in agreement with the picture of pseudo-chains formed by groups of microparticles and contact resistances between them.

The results of fitting indicate that R_{E-CH} is negligible. This is a conclusion, not a hypothesis. That is, R_{E-CH} is kept in the general expression used to model the experimental data, which can be made without introducing any complication. After fitting it is confirmed the prediction of Eq. (2): R_{E-CH} is very low and negligible in comparison with the other contributions to R in the considered range of stresses.

As already mentioned, the value of γ is defined by the electron effective mass, m , and the tunnelling barrier, ϕ . These parameters are heavily dependent on the chemical and structural nature of the fillers and polymer matrix. Since γ determines the recovered values of n , x_o and l , then simulations of these parameters were performed as function of γ (Figure 8). The variable m was varied in the range $(0.5 - 1.5)m_e$ while ϕ between $(0.5 - 1.5) \text{ eV}$. For these ranges, γ varies between $(0.5 - 1.5) \times 10^{10} \text{ m}^{-1}$. It is observed in Fig. 8 that l and n vary appreciably (about 2 orders of magnitude). On the other hand, x_o remains between 0.6 and 2.1 nm, approximately. This indicates that although a precise determination of n and l requires accurate measurements of γ , the model predicts values of x_o which are within the typical scale for electronic tunnelling.⁹

5 Influence of the matrix elasticity, E , filler-polymer tunnelling barrier, ϕ , and average tunnelling distance, x_o , on $R_{tunnel}(P)$

In this section the influence of key parameters that are essential for designing piezoresistive anisotropic stress sensors based on SECs is explored via numerical calculation. To simplify the analysis, the Neo-Hooke dependence between λ and P is assumed. It is assumed also that the surfaces between tunnels are planes, then $R_{tunnel}(P)$ is given by the original Simmons expression: $R_{tunnel} \propto \frac{x}{B\gamma} \exp(\gamma x)$. Therefore, a simplified expression of $\frac{R_{tunnel}}{R_{tunnel(0)}}$ as a function of P is presented based on the developed model [Eqs. (19)], where $R_{tunnel(0)} \equiv R_{tunnel}(P = 0)$. Although that expression assumes a simple dependence of x with P , it does contain the essential physics. If these approximations are considered together, neglecting the contribution of R_{E-CH} and assuming that n and N do not change by application of P , from Eq.(3) it is

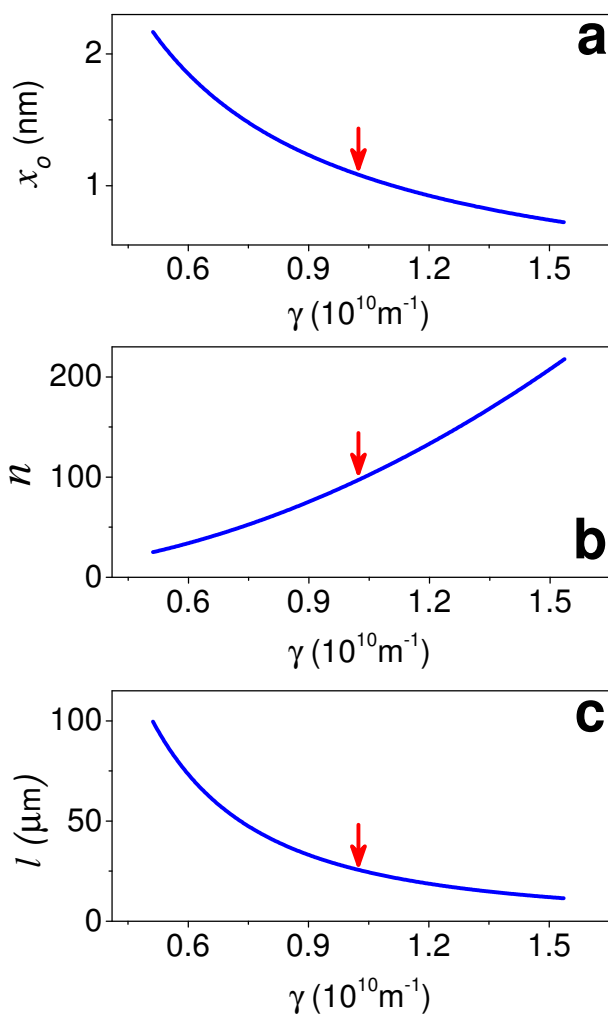


Fig. 8 Simulations of x_o , n and l as function of γ using the values $A_1 = (2.2 \pm 0.2)\Omega$, $A_2 = \gamma x_o = (11.1 \pm 0.5)$ and $A_3 = (0.47 \pm 0.07)\Omega$ (reference SEC sample). The arrow indicates γ^\dagger .

obtained:

$$\frac{R - R(\infty)}{R_o - R(\infty)} \approx \frac{R_{\text{tunnel}}}{R_{\text{tunnel}(0)}} = \lambda \exp[\gamma x_o (\lambda - 1)] \quad (19)$$

where $R_o \equiv R(P = 0)$ and $R(\infty) \equiv R(P \rightarrow \infty)$. For simplicity, in this Section λ is calculated as $\lambda^{N-H}(P; E)$, given by the Neo-Hook model [Equations (13)-(15)] with $C_1^{N-H} = E/6$. Thus, the above relationship shows that $\frac{R_{\text{tunnel}}}{R_{\text{tunnel}(0)}}$ depends only on the applied stress relative to the Young's modulus of the polymer matrix, P/E , and on the initial separation between chains relative to γ^{-1} , $x_o\gamma$. Figure 9-a illustrates simulated curves of $\frac{R_{\text{tunnel}}}{R_{\text{tunnel}(0)}}$ for different values of E at fixed $x_o\gamma$, while the influence of $x_o\gamma$ at fixed E is shown in Fig. 9-b.

Figure 9-a shows that when polymers with increasing values

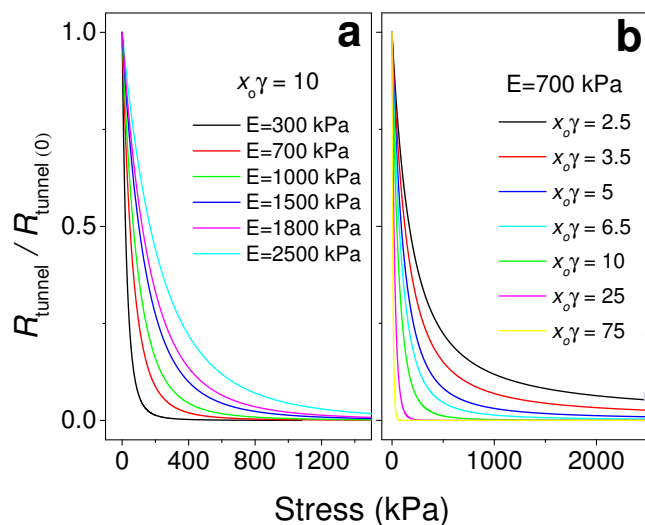


Fig. 9 Simulated curves for the effect of (a) Young modulus of the unfilled polymeric matrix, E , for $x_o\gamma = 10$ and (b) $x_o\gamma$ with $E = 700$ kPa on $\frac{R_{\text{tunnel}}}{R_{\text{tunnel}(0)}}$. The curves were calculated using Eq. (19) with $\lambda = \lambda^{N-H}(P; E)$.

of E are considered, then larger stresses are required in order to achieve a given average tunnelling gap, $x(P)$, and hence the same $\frac{R_{\text{tunnel}}}{R_{\text{tunnel}(0)}}$, an expected behaviour retained by the affine assumption. It is worth noting that the Young's modulus of the PDMS matrix can be increased by increasing the amount of cross-linking agent in the matrix without changing appreciably the potential barrier, ϕ , that is, without changing $x_o\gamma$.

Analogously, Fig. 9-b shows that fixing x_o and E , higher stresses are required to achieve the same percentage decrease in R_{tunnel} for lower values of γ , for example using a filler-matrix couple with lower values of ϕ . Thus, Eq. (19) and Figure 9 remark that the sensitivity and measurement range of stress sensor based on SECs can be modified by changing the elasticity of the polymer matrix (changing the amount of cross-linking agent), the average separation between chains (changing the curing conditions, such as the magnitude and exposition time of $\mathbf{H}_{\text{curing}}$) and the potential barrier (using different filler-matrix couples). Finally, it must be noted that no inflection points are predicted by the model for the piezoresistive response of SECs. This is a significant difference in comparison with the response observed in some isotropic filler-elastomer composites prepared in our group⁴⁷ where no pseudo-chains are created.

Conclusions

The presented model describes very well the experimental piezoresistivity observed in the anisotropic structured elastomer composites (SEC). The analysis of the parameters suggests that pseudo-chains have multiple gaps. The existence of gaps is in

agreement with the concept of pseudo-chains instead of compact chains. Optical photographs and SEM images confirm the formation of pseudo-chains that are not compact but present irregular arrangements of individual filler's particles, which generates relatively large gaps between particles. The model predictions are in concordance with the presence of those gaps inside the pseudo-chains combined with electron tunnelling through the gaps. The results also indicate that the intrinsic resistance between gaps can be considered constant (independent of P) with good approximation. The model predicts a non-linear relationship between R and P . The only input required is the stress-strain curve of the unfilled polymer matrix (not of the SEC) and the number of columns that go across the SEC sample (N). Then, three fitting parameters are recovered, A_1 , A_2 and A_3 , when fitting the experimental results, which are related to microscopic variables (γ , x_o , n and l). The model predicts that for a given couple filler-polymer the parameter γ has no sensitivity (or very low) to the experimental conditions used for preparing the SECs but x_o (the distance for tunnelling at $P = 0$) is expected to be very dependent of experimental factors such as the concentration of fillers, magnitude and exposition time of H_{curing} , degree of cross-linking, etc. The model predicts also that if x_o is relatively low (at fixed γ) then a large dynamic range of P is required in order to observe a large relative change of R (Figure 9-b). Numerical calculations using simplified expressions confirm that a required extended dynamic range of stresses for systems with larger Young's modulus, E , is required, which is reasonable expected from basic considerations of the elastic behaviour (Figure 9-a).

Acknowledgements

RMN and PIT are research members of the National Council of Research and Technology (CONICET, Argentina). Financial support was received from UBA (UBACyT projects 2012-2015, number 20020110100098 and 2011-2014 number 20020100100741) and from the Ministry of Science, Technology, and Innovation (MINCYT-FONCYT, Argentina, PICT 2011-0377). Support from the Center of Documental Production (CePro) and the Center of Advanced Microscopy (CMA) (FCEyN, UBA) to obtain the shown SEM-TEM images and from the Low-Temperatures Laboratory (Department of Physics, FCEyN, UBA) to implement the device used to generate the structured materials is gratefully acknowledged.

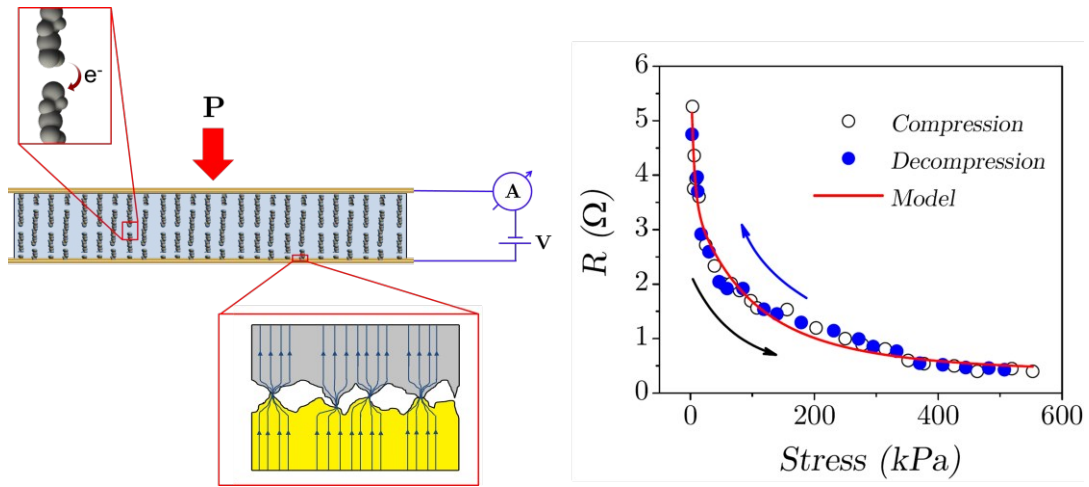
References

- 1 M. M. Ruiz, M. Claudia Marchi, O. E. Perez, G. E. Jorge, M. Fascio, N. D'Accorso and R. Martín Negri, *Journal of Polymer Science Part B: Polymer Physics*, 2015, **53**, 574–586.
- 2 M. M. Ruiz, J. L. Mietta, P. S. Antonel, O. E. Pérez, R. M. Negri and G. Jorge, *Journal of Magnetism and Magnetic Materials*, 2013, **327**, 11–19.

- 3 K. Shahrivar and J. de Vicente, *Soft Matter*, 2013, **9**, 11451–11456.
- 4 Z. Varga, G. Filipcsei and M. Zrínyi, *Polymer*, 2006, **47**, 227–233.
- 5 J. L. Mietta, M. M. Ruiz, P. S. Antonel, O. E. Perez, A. Butera, G. Jorge and R. M. Negri, *Langmuir*, 2012, **28**, 6985–6996.
- 6 J. L. Mietta, G. Jorge, O. E. Perez, T. Maeder and R. M. Negri, *Sensors and Actuators A: Physical*, 2013, **192**, 34–41.
- 7 J. L. Mietta, G. Jorge and R. M. Negri, *Smart Materials and Structures*, 2014, **23**, 085026.
- 8 E. Coquelle and G. Bossis, *Journal of Advanced Science*, 2005, **17**, 132–138.
- 9 N. Kchit and G. Bossis, *Journal of Physics D: Applied Physics*, 2009, **42**, 105505.
- 10 N. Kchit, P. Lancon and G. Bossis, *Journal of Physics D: Applied Physics*, 2009, **42**, 105506.
- 11 J. L. Mietta, R. M. Negri and P. I. Tamborenea, *The Journal of Physical Chemistry C*, 2014, **118**, 20594–20604.
- 12 G. Filipcsei, I. Csetneki, A. Szilágyi and M. Zrínyi, *Oligomers-Polymer Composites-Molecular Imprinting*, Springer, 2007, pp. 137–189.
- 13 A. Butera, N. Álvarez, G. Jorge, M. Ruiz, J. Mietta and R. Negri, *Physical Review B*, 2012, **86**, 144424.
- 14 T. Liu, X. Gong, Y. Xu, S. Xuan and W. Jiang, *Soft Matter*, 2013, **9**, 10069–10080.
- 15 D. Günther, D. Y. Borin, S. Günther and S. Odenbach, *Smart Materials and Structures*, 2012, **21**, 015005.
- 16 T. Gundermann and S. Odenbach, *Smart Materials and Structures*, 2014, **23**, 105013.
- 17 Y. Hou, D. Wang, X.-M. Zhang, H. Zhao, J.-W. Zha and Z.-M. Dang, *Journal of Materials Chemistry C*, 2013, **1**, 515–521.
- 18 M. Mohiuddin, *PhD thesis*, Concordia University, 2012.
- 19 J. Ku-Herrera, F. Avilés and G. Seidel, *Smart Materials and Structures*, 2013, **22**, 085003.
- 20 J. E. Mark, *Physical properties of polymers handbook*, Springer, 1996.
- 21 Y. Lau and W. Tang, *Journal of Applied Physics*, 2009, **105**, 124902.
- 22 M. R. Gomez, D. M. French, W. Tang, P. Zhang, Y. Lau and R. Gilgenbach, *Applied Physics Letters*, 2009, **95**, 072103.
- 23 P. Zhang and Y. Lau, *Journal of Applied Physics*, 2010, **108**, 044914.
- 24 E. Holm, J. Williamson and R. Holm, *Electric Contacts: Theory and Application*, Springer Berlin Heidelberg, 2010.
- 25 P. Zhang, Y. Lau, W. Tang, M. Gomez, D. French, J. Zier and R. Gilgenbach, *Electrical Contacts (Holm)*, 2011 IEEE 57th Holm Conference on, 2011, pp. 1–6.
- 26 P. Zhang, *PhD thesis*, The University of Michigan, 2012.

- 27 G. Samsonov, *Handbook of the Physicochemical Properties of the Elements*, Springer US, 2012.
- 28 S. Stassi, V. Cauda, G. Canavese and C. F. Pirri, *Sensors*, 2014, **14**, 5296–5332.
- 29 X.-W. Zhang, Y. Pan, Q. Zheng and X.-S. Yi, *Journal of Polymer Science Part B: Polymer Physics*, 2000, **38**, 2739–2749.
- 30 M. Kalantari, J. Dargahi, J. Kollvecses, M. G. Mardasi and S. Nouri, *Mechatronics, IEEE/ASME Transactions on*, 2012, **17**, 572–581.
- 31 G. Ambrosetti, C. Grimaldi, I. Balberg, T. Maeder, A. Danani and P. Ryser, *Physical Review B*, 2010, **81**, 155434.
- 32 M. Sureshkumar, H. Y. Na, K. H. Ahn and S. J. Lee, *ACS applied materials & interfaces*, 2015, **7**, 756–764.
- 33 S. Gong and Z. H. Zhu, *Polymer*, 2014, **55**, 4136–4149.
- 34 J. Park, Y. Lee, J. Hong, M. Ha, Y.-D. Jung, H. Lim, S. Y. Kim and H. Ko, *ACS nano*, 2014, **8**, 4689–4697.
- 35 C. Li, E. T. Thostenson and T.-W. Chou, *Applied Physics Letters*, 2007, **91**, 223114.
- 36 J. G. Simmons, *Journal of Applied Physics*, 1964, **35**, 2655–2658.
- 37 C. Chen, *Introduction to Scanning Tunneling Microscopy*, OUP Oxford, 2008.
- 38 C. Jin and K. S. Thygesen, *Physical Review B*, 2014, **89**, 041102.
- 39 X. Ma, Q. Shu, S. Meng and W. Ma, *Thin solid films*, 2003, **436**, 292–297.
- 40 T. Kathriner, *Diploma Thesis*, ETH Zürich, 2008.
- 41 D. Ivaneyko, V. Toshchevikov, M. Saphiannikova and G. Heinrich, *Soft matter*, 2014, **10**, 2213–2225.
- 42 J. Domurath, M. Saphiannikova, G. Ausias and G. Heinrich, *Journal of Non-Newtonian Fluid Mechanics*, 2012, **171**, 8–16.
- 43 Y.-S. Yu and Y.-P. Zhao, *Journal of colloid and interface science*, 2009, **332**, 467–476.
- 44 W. Graessley, *Polymeric Liquids and Networks*, Taylor & Francis, 2003.
- 45 R. Nickalls, *The Mathematical Gazette*, 2009, 66–75.
- 46 M. Amjadi, A. Pichitpajongkit, S. Lee, S. Ryu and I. Park, *ACS nano*, 2014, **8**, 5154–5163.
- 47 R. M. Negri, S. D. Rodriguez, D. L. Bernik, F. V. Molina, A. P. Ilosos and O. Perez, *Journal of Applied Physics*, 2010, **107**, 113703.

Graphical Abstract



A constitutive model for the total anisotropic reversible piezoresistivity in PDMS/magnetite-silver structured elastomer composite is proposed.